Applied Physics Letters

Direct laser writing of complex microtubes using femtosecond vortex beams

Cite as: Appl. Phys. Lett. **110**, 221103 (2017); https://doi.org/10.1063/1.4984744
Submitted: 28 January 2017 . Accepted: 18 May 2017 . Published Online: 31 May 2017

Liang Yang, Dongdong Qian, Chen Xin, Zhijiang Hu, Shengyun Ji, Dong Wu, Yanlei Hu, Jiawen Li, Wenhao Huang, and Jiaru Chu

View Online Export Citation CrossMark

ARTICLES YOU MAY BE INTERESTED IN

Dielectric geometric phase optical elements fabricated by femtosecond direct laser writing in photoresists
Applied Physics Letters **110**, 181101 (2017); https://doi.org/10.1063/1.4982602

Optical superimposed vortex beams generated by integrated holographic plates with blazed grating
Applied Physics Letters **111**, 061901 (2017); https://doi.org/10.1063/1.4997590

Waveform control of enhanced THz radiation from femtosecond laser filament in air
Applied Physics Letters **110**, 221102 (2017); https://doi.org/10.1063/1.4984599

© 2017 Author(s).

Direct laser writing of complex microtubes using femtosecond vortex beams

Liang Yang, Dongdong Qian, Chen Xin, Zhijiang Hu, Shengyun Ji, Dong Wu,[a] Yanlei Hu, Jiawen Li, Wenhao Huang, and Jiaru Chu
CAS Key Laboratory of Mechanical Behavior and Design of Materials, Department of Precision Machinery and Precision Instrumentation, University of Science and Technology of China, Hefei 230026, People's Republic of China

(Received 28 January 2017; accepted 18 May 2017; published online 31 May 2017)

Microfabrication by using structured laser beams provides a rapid and facile way for creating some specific microstructures. As an important member in the structured beam category, optical vortices can be easily generated by a helical phase and focused into a geometry-tunable pattern by an objective. In this work, optical vortices with diverse intensity distributions, e.g., different sizes, geometries, and deflection angles, are generated by controlling the phase factors imprinted on optical vortices, including topological charge, fold number, and modulation depth, respectively. The focusing properties of the measured optical vortices in a high numerical aperture laser microfabrication system agree with the theoretical calculation by the Debye vectorial diffraction theory. Three dimensional complex microtubes are rapidly realized by simply scanning the optical vortices along a designed route in a photoresist. With this method, microtubes with controlled diameters, polygonal geometry, winding edges, and even 3D spiral microtubes are facilely achieved. *Published by AIP Publishing.*
[http://dx.doi.org/10.1063/1.4984744]

Femtosecond two-photon polymerization (TPP) based on a structured laser beam by using a spatial light modulator (SLM) has become a hot topic because it can significantly decrease the fabrication time and enhance the efficiency of conventional point-to-pint scanning.[1] Until now, some very specific distributions, including multiple beam spot arrays,[2–5] Bessel beams,[6] spatially shifted vortex beams,[7] double-helix beams,[8] and ring laser beams,[9] have been explored for parallelization of the direct laser writing or even single-shot microfabrication.

Optical vortices are a kind of specific beams with azimuthal phase variation patterns, which have been widely used in optical tweezers, stimulated emission depletion (STED) lithography, surface structuring, micromachining, and photopolymerization. In contrast to Bessel beams, shifted vortex beams, and double-helix beams in previous works, optical vortices have more controllable parameters, including topological charge l, fold number m, and modulation depth α, which means that the laser pattern can be more flexibly structured. In the optical tweezer technique, orbital angular momentum of optical vortices exerts torques on objects for effective trapping,[10] which has widespread applications in micromechanics[11] and biotechnology.[12] In STED lithography, optical vortices have been used to achieve spatial resolution beyond optical diffraction limits by depleting the fluorophores around a desired area.[13] Femtosecond vortex beams can also lead to interesting ridges, wrinkles, and pores on the material surface,[14,15] which are not achievable by the standard beams with a Gaussian intensity profile. Laser machining by optical vortices showed the ability to create unique material structures, like microneedles on the metal surface,[16] microcavities on soda-lime glass,[17] and circular polymer microstructures.[18–20] Although optical vortices present broad and significant applications in the above areas, the potential of using optical vortices in femtosecond laser TPP is far from fully exploited. No quantitative study has been done on how the modulation and focusing properties of optical vortices affect the microstructure fabrication. Systematic research on manipulating optical vortices for rapid fabrication of controllable micro/nano-structures remains to be conducted.

In this paper, optical vortices are generated by imprinting a helical phase on an incident femtosecond laser beam using a liquid crystal phase only SLM. The focusing properties of optical vortices are investigated with the Debye vectorial diffraction theory. How the phase factors imprinted on the optical vortex, including topological charge l, fold number m, and modulation depth α, affects its intensity distribution is theoretically and experimentally studied. Microtubes are fabricated by simply scanning the optical vortices along a designed route in the photoresist. Furthermore, the relationship between phase factors and microtube parameters is quantitatively studied. The diameters, polygonal geometry, and deflection angle of edges of fabricated microtubes are well controlled by modulating the phase factors of the optical vortex. On this basis, microtubes with controllable geometry parameters and even 3D spiral microtubes are easily achieved.

The experimental setup is schematically illustrated in Fig. 1(a). A femtosecond laser source with a wavelength of 780 nm (Chameleon Ultra, Coherent GmbH; repetition rate: 80 MHz; pulse width: <140 fs) was used for the TPP process. After expansion, the laser beam illuminates an SLM (Pluto NIRII, Holoeye, 1920 × 1080 pixels, 256 grey levels, and pixel pitch of 8 μm), on which phase mask is encoded [inset of Fig. 1(a)]. The modified beam is relayed to the input pupil of a high numerical aperture (NA) objective lens (60×, NA = 1.35, Olympus). The optical vortex is focused and diverged along the propagation direction [Fig. 1(b)]. A vortex pattern is prototyped by TPP with a single exposure of

[a]Author to whom correspondence should be addressed: dongwu@ustc.edu.cn

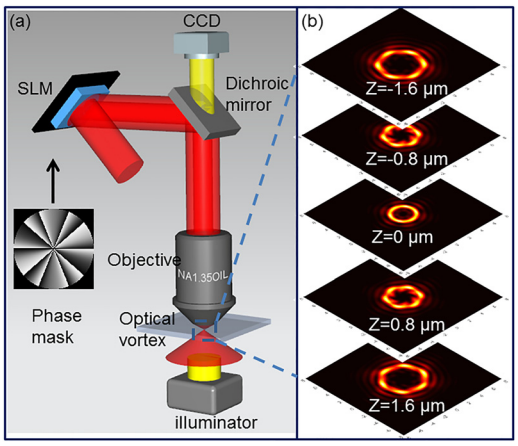

FIG. 1. Creation of the femtosecond vortex beam for direct laser writing of microtubes. (a) Schematic diagram of the experimental setup. (b) Simulated intensity distribution in the propagation direction in the focus region of an objective with a numerical aperture of 1.35.

photoresist (SZ2080) sample anchored to a 3D piezo stage (E545, Physik Instrument). Microtubes are fabricated by simply scanning the focused optical vortex along a predesigned 3D route, which is realized by controlling the movement of the 3D piezo stage with a computer. SZ2080 is a solid material in TPP microfabrication, which is prebaked at 100 °C for 1 h. The absorption band is located in the spectral range of 300–400 nm with the absorption peak at 380 nm. The refractive index of the material is ~1.523 at 632.8 nm.[21]

The optical vortex with the helical mode is formed by imprinting a phase factor, $\exp(il\varphi)$, onto a Gaussian beam, where φ is the azimuthal angle around the optical axis and l is the topological charge, an integer characterizing an l-fold helix. The beam intensity is distributed into a ring with radius R_l at the focal point. When R_l varies with φ, a more complex Lissajous intensity pattern can be obtained in the focal plane. This is realized by the imprint phase factor $\phi(l,\varphi) = \exp\{il[\varphi + \alpha\sin(m\varphi + \beta)]\}$ onto the incident Gaussian beam.[10] In the experiment, a blazed grating pattern is directly added with the hologram for optical vortex generation to separate the optical vortex from zero diffraction order, which is filtered before entering the objective. The characteristic of the Lissajous pattern is controlled by four factors. In particular, l determines the local radius of maximum intensity at angle φ, α controls the depth of modulation, m produces an m-fold symmetric pattern, and β determines the orientation of the pattern.

For direct laser writing of microstructures, the optical vortex needs to be tightly focused with a high NA objective. Hence, it is crucial to investigate the focusing properties of the optical vortex. Different from the scalar diffraction theory, the vectorial diffraction behavior of light passing through a high NA objective is accounted with the Debye vectorial diffraction theory for better calculation of the intensity distribution in the focal region.[22] Since the paraxial approximation does not consider the vectorial nature, in this study, we use the Debye vectorial diffraction theory,[23] which describes the depolarization effect of a high-NA objective by calculating the three orthogonal field components Ex, Ey, and Ez. By the Debye vectorial diffraction theory, the optical intensities near the focal spot are derived as[24]

$$\boldsymbol{E}(x_2,y_2,z_2) = -\frac{iC}{\lambda}\int_0^{\alpha}\int_0^{2\pi} \sin\theta \boldsymbol{E}_{obj}(\theta,\varphi)\sqrt{\cos\theta}\boldsymbol{P}(\theta,\varphi) \times \exp\left[ikn(z_2\cos\theta + x_2\sin\theta\cos\varphi + y_2\sin\theta\sin\varphi)\right]d\theta d\varphi, \quad (1)$$

where C is a constant, $\boldsymbol{E}_{obj}(\theta,\varphi)$ is the electric field at the entrance pupil of the objective, $k = 2\pi/\lambda$ is the wave number of incident light, n is the refractive index of the immersion medium, θ represents the focusing angel of the objective lens, and φ is the azimuthal angle of the object plane. α is the maximum focusing angle of the objective lens and can be calculated according to the formula: $\alpha = \arcsin(NA/n)$, where NA is the numerical aperture of objective lens. $\boldsymbol{P}(\theta,\varphi)$ represents the polarization state of the EM field in the focal region, which can be rewritten as

$$\boldsymbol{P}(\theta,\varphi) = \left[1 + (\cos\theta - 1)\cos^2\varphi\right]\boldsymbol{i} + \left[(\cos\theta - 1)\cos\varphi\sin\varphi\right]\boldsymbol{j} - (\sin\theta\cos\varphi)\boldsymbol{k} \quad (2)$$

for incidence with linear polarization in the X direction.

To show the effects of phase factors on the microstructure fabrication, theoretical simulations and experiments are conducted. We started by controlling the topological charge l (Fig. 2), while fixing $m = 1$, $\alpha = 0.04$, and $\beta = 0$, without the loss of generality. The phase factors m, α, and β can also be changed to other values. Optical vortices show circular intensity distribution at the focal plane [Fig. 2(b)] and diverge quickly along the propagation direction [Fig. 2(c)]. The diameter of the intensity pattern at the focal plane increases as the topological charge is changed from $l = 2$ to $l = 20$ [Fig. 2(a)]. In the experiment, the optical vortex is projected into a photoresist sample, and complex 2D patterns can be fabricated by a single exposure without need of point to point scanning. All the microstructures are fabricated with a single exposure of 50 ms, with a laser power of 80 mW measured in front of the objective [Fig. 2(d)]. The increase in the diameter

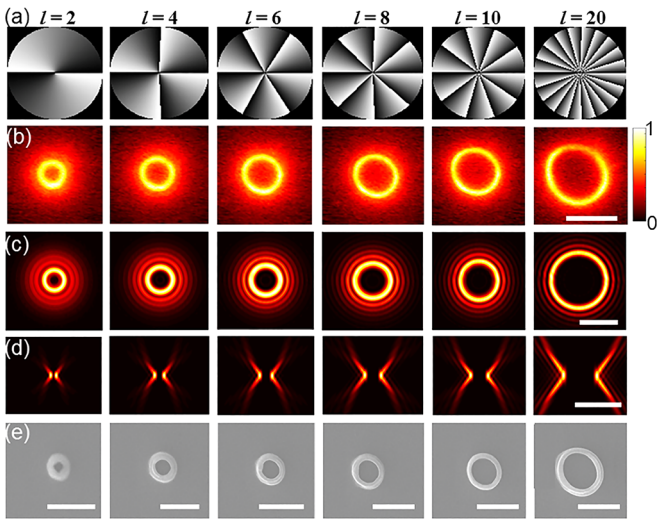

FIG. 2. TPP by femtosecond optical vortices with topological charge from $l = 2$ to $l = 20$. (a) Phase masks for optical vortices with different topological charges. (b) Measured and (c) calculated intensity distribution at the focus plane. (d) Calculated intensity distribution along the beam propagation direction. (e) All the circular structures are two-photon polymerized with a single exposure of 50 ms by 80 mW laser power. All the scale bars are 5 μm.

matches well with the theoretical calculation. The quantitative study of the diameter control will be discussed in detail [Fig. 4]. We can find that the microstructures are not perfectly homogeneously polymerized. This is attributed to two reasons. First, both the pixelization of holograms and the non-ideality of the optical system in the experiment may bring aberrations to the optical vortex. Second, the optical vortex exhibits an inhomogeneous intensity distribution around the inner circle after high NA focusing for linear polarization incidence, as the case in our experiment. For better resolution and uniformity of fabricated microstructures, the aberration of high NA fabrication systems can be compensated by controlling the point-spread-function of the focal pattern with optimized hologram generating algorithms.[25–27]

Fold number m and modulation depth α affect the number and deflection angle of edges of the polymerized microstructure. By modulating m and α, more complex 2D microstructures (Fig. 3) can be fabricated with single exposure. When changing m, polygonal optical vortices are generated, as calculated [Fig. 3(a)] and measured using a CCD camera [Fig. 3(b)]. Correspondingly, the fabricated structures with $m = 2$, 3, 4, 5, 6, and 10 exhibit elliptical, triangular, square, pentagonal, hexagonal, and decagonal geometries [Fig. 3(c)]. It is found by both the calculation and the experiment that the intensity distribution is not homogeneous along the edges of the polygonal pattern and is stronger at the junction of edges. This inhomogeneous intensity distribution directly leads to the nonuniform wall thickness of the polymerized polygonal pattern. In the experiment, the phase factors l, α, and β are fixed to be $l = 10$, $\alpha = 0.04$, and $\beta = 0$, without the loss of generality. Similarly, by controlling the α from 0.02 to 0.20, while keeping phase factors to be $l = 10$, $m = 6$, and $\beta = 0$ [Fig. 3(d)] without the loss of generality,

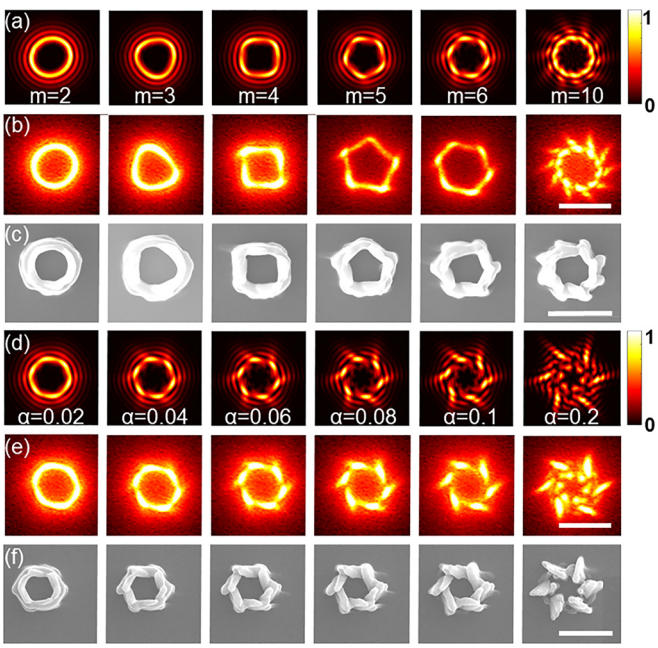

FIG. 3. TPP with femtosecond optical vortices by controlling fold number m and modulation depth α. (a) and (d) Calculated intensity distribution at the focus plane of objective with m varies from 2 to 10 and α varies from 0.02 to 0.20. (b) and (e) Measured optical vortices at the focal plane of the objective. (c) and (f) SEM images of polymerized polygonal microstructures by single exposure of femtosecond optical vortices. The scale bars are 5 μm.

hexagonal optical vortices with different deflection angles are realized [Fig. 3(e)]. The optical vortex and the polymerized microstructure [Fig. 3(f)] evolve from standard hexagon to a pattern with six sidelobes, and the sidelobes' deflection angle increases with α, which agrees well with the theoretical calculation. All the microstructures in Figs. 3(c) and 3(f) are fabricated with an exposure time of 500 ms and a laser power of 80 mW.

For the precise control of the size and geometry of microstructures, a quantitative study (Fig. 4) on the dependence of microstructure geometry on the topological charge l and modulation depth α is conducted (fold number m only controls the edge number of microstructure). When topological charge l varies from 2 to 20, the outside diameter varies from 2.4 μm to 5.4 μm and the inner diameter varies from 0.9 μm to 4.3 μm [Fig. 4(a)]. Other phase factors are fixed to be $m = 1$, $\alpha = 0.04$, and $\beta = 0$. The diameter can be controlled approximately linearly by changing l. When topological charge l is further decreased to 1, the inner diameter can reach down to a minimum value of ~600 nm. The inset of Fig. 4(a) shows the intensity distribution of a focused optical vortex and the white curve is the intensity cross section along the X direction. The outer and inner diameters of the optical vortex are calculated according to the half height full width of the intensity distribution. The deflection angle θ of sidelobes is defined as shown in the inset of Fig. 4(b) and increases approximately linearly with phase factor α, when fixing $l = 10$, $m = 6$, and $\beta = 0$. When $\alpha < 0.1$, the change in the deflection angle θ is smaller than 15^0 and the polymerized microstructure keeps a hexagonal geometry. However, when $\alpha > 0.1$, the deflection angle becomes obvious and the polymerized microstructure shows a wind wheel geometry [the rightmost image of Fig. 3(f)]. The scale bars are from the variance of measurements. The deviation between measured and calculated values comes from two aspects. First, one significant reason for the discrepancy between the measured and calculated values is the shrinkage of photoresist in the development process. The shrinkage of the polymerized microstructure leads to smaller measured inner and outer diameters than the theoretical simulation [Fig. 4(a)], especially when the laser exposure dosage is close to the photoresist polymerization threshold. The shrinkage also results in the deformation of the microstructure, which explains the deviation between measured and calculated unfolding angles of sidelobes [Fig. 4(b)]. Second, the calculation is conducted on a series of assumptions including standard Gaussian incidence, ideal optical system, and ignorable refractive index mismatch behind the objective. In fact, the pixelization of holograms, the non-ideality of the optical system, the high NA objective system, and the mismatch of the refractive index will all bring aberration to the focused optical vortex pattern and lead to the deviation of calculation from the actual situation.

Based on the preceding systematic study on TPP with the optical vortex, an approach for rapid fabrication of 3D microtubes is proposed. Microtubes can be fabricated flexibly by simply scanning femtosecond optical vortices along a designed route (Fig. 5). Different from the conventional TPP process where microtubes are fabricated by the overlapping of single voxels, microtubes are achieved by rapid scanning

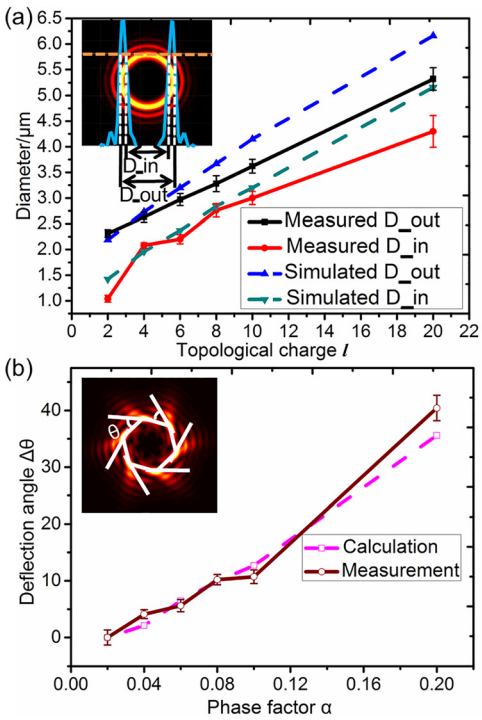

FIG. 4. (a) Dependence of the diameter of the polymerized circular microstructure on topological charge l. The inset shows that the inner and outer diameters of optical vortices are calculated according to the half height full width of the intensity distribution. (b) Relationship between the change of deflection angle $\Delta\theta$ and modulation depth α. The inset shows the definition of deflection angle θ.

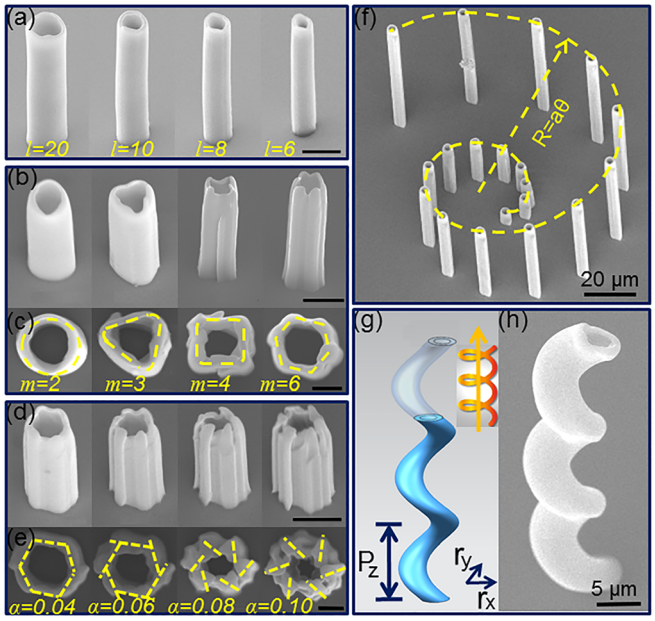

FIG. 5. Complex microtubes fabricated by direct laser writing using femtosecond vortex beams. (a) Microtubes with controllable diameter by changing topological charge l. (b) and (c) Microtubes with elliptical, triangular, square, and hexagonal geometries by controlling fold number m. (d) and (e) Hexagonal microtubes fabricated by changing modulation α from 0.04 to 0.06, 0.08, and 0.10 (from left to right). (f) 3D "Archimedes spiral" microtube array with height increasing linearly. (h) Spiral microtubes with precisely designed size and period fabricated according to the scanning route in (g), which is difficult for previous microtube fabrication techniques. The scale bars are 5 μm in (a), (b), (d), and (h), 2 μm in (c) and (e), and 20 μm in (f).

of optical vortices. Thus, fabrication time can be significantly reduced by two orders of magnitude. Additionally, the size and geometry of microtubes can be controlled flexibly by changing topological charge l, fold number m, and modulation depth α. Figure 5(a) shows the SEM images of circular microtubes with gradient diameter by changing topological charge l from 20 to 10, 8, and 6. The scanning speed for all circular microtubes fabrication is 50 μm/s, while the used laser power is 80 mW, 50 mW, 40 mW, and 30 mW, respectively. The microtubes are 30 μm high and the fabrication time is 0.6 s, while it increases to 270 s for conventional single spot direct laser writing with a piezo stage. Figures 5(b) and 5(c) show elliptical, triangular, square, and hexagonal microtubes by controlling fold number m. In theory, polygonal microtubes with an arbitrary number of edges can be fabricated, but as the edge number increases, the polygonal microtube is more close to a circular microtube. Similarly, by controlling modulation depth α, microtubes with winding edges are realized [Figs. 5(d) and 5(e)]. The hexagonal microtubes are fabricated by fixing $l = 16$ and $m = 6$ and changing α from 0.04 to 0.06, 0.08, and 0.10. The scanning speed for all polygonal microtubes' fabrication is 50 μm/s and the used laser power is 75 mW. Inhomogeneous polymerization can be found in Figs. 5(b)–5(e), which is attributed to the aberration of the focused optical vortex caused by the optical system. The aberration needs to be effectively compensated if more homogeneous polymerization is expected. Specially, an "Archimedes spiral" microtube array with increasing heights from 5 μm to 150 μm is designed and fabricated with a laser power of 50 mW and a scanning speed of 40 μm/s, by the optical vortex with $l = 10$, $m = 1$, and $\alpha = 0.02$ [Fig. 5(f)]. This is difficult for previous microtube fabrication techniques, such as 2D UV photolithography,[28] template based microtube fabrication,[29] and self-rolling technique.[30] Besides straight microtubes, complex 3D microtubes can be easily realized by scanning optical vortices along a designed 3D route. Figure 5(h) shows the SEM image of a 3D spiral microtube scanned with a strategy illustrated in Fig. 5(g). The spiral diameters in x and y directions r_x and r_y are 2 μm and the period in the z direction P_z is 20 μm. The optical vortex with $l = 20$, $m = 1$, and $\alpha = 0.02$ is adopted for the fabrication of spiral microtubes, and a laser power of 50 mW and a scanning speed of 40 μm/s are used. Such microtubes are of great interest for the construction of micro-optics,[31] biomedical devices,[30] micro-fluidics,[32] micro-pumps,[29] micro-sensors,[32] and lab on a tube devices.[30]

In conclusion, we have theoretically investigated the focusing properties of optical vortices generated by phase modulation with the Debye vectorial diffraction theory. Direct laser writing of 3D microtubes is realized using the focused optical vortices. In contrast to the commonly used single spot scanning technique, microtubes are facilely and rapidly fabricated by scanning the optical vortices along a designed route. Furthermore, the size (from 0.6 μm to 4.3 μm), geometry (e.g., elliptical, triangular, square, and hexagonal), and deflection angle of edges of fabricated microtubes can be precisely controlled by modulating the topological charge l, fold number m, and modulation depth α of optical vortices. This research takes advantage of the flexibility of phase modulation and the high precision of direct laser writing, leading to a method for rapid

fabrication of varied micro/nano-tubes. It may inspire new thoughts of high-efficient fabrication of functional devices.

This work was supported by the National Natural Science Foundation of China (Nos. 51675503, 61475149, 51405464, 61675190, and 51605463), the Fundamental Research Funds for the Central Universities (Grant Nos. WK2480000002 and WK2090000011), the China Postdoctoral Science Foundation (Grant Nos. 2016M590578 and 2016M602027), Chinese Academy of Sciences Instrument Project (YZ201566), and "Chinese Thousand Young Talents Program."

[1]J. K. Hohmann, M. Renner, E. H. Waller, and G. Freymann, Adv. Opt. Mater. **3**, 1488 (2015).
[2]L. Yang, A. El-Tamer, U. Hinze, J. W. Li, Y. L. Hu, W. H. Huang, J. R. Chu, and B. N. Chichkov, Opt. Laser Eng. **70**, 26 (2015).
[3]K. Obata, J. Koch, U. Hinze, and B. N. Chichkov, Opt. Express **18**, 17193 (2010).
[4]A. Jesacher and M. J. Booth, Opt. Express **18**, 21090 (2010).
[5]E. H. Waller and G. von Freymann, Opt. Express **21**, 21708 (2013).
[6]R. J. Winfield, B. Bhuian, S. O'Brien, and G. M. Crean, Appl. Phys. Lett. **90**, 111115 (2007).
[7]H. Lin and M. Gu, Appl. Phys. Lett. **102**, 084103 (2013).
[8]S. Zhang, Y. Li, Z. Liu, J. Ren, Y. Xiao, H. Yang, and Q. Gong, Appl. Phys. Lett. **105**, 061101 (2014).
[9]C. Zhang, Y. Hu, J. Li, G. Li, J. Chu, and W. Huang, Opt. Express **22**, 3983 (2014).
[10]J. E. Curtis and D. G. Grier, Opt. Lett. **28**, 872 (2003).
[11]X. Lin, G. Hu, Q. Chen, L. Niu, Q. Li, A. Ostendorf, and H. Sun, Appl. Phys. Lett. **101**, 113901 (2012).
[12]G. D. M. Jeffries, J. S. Edgar, Y. Zhao, J. P. Shelby, C. Fong, and D. T. Chiu, Nano Lett. **7**, 415 (2007).
[13]J. Fischer and M. Wegener, Laser Photon. Rev. **7**, 22 (2013).
[14]K. K. Anoop, A. Rubano, R. Fittipaldi, X. Wang, D. Paparo, A. Vecchione, L. Marrucci, R. Bruzzese, and S. Amoruso, Appl. Phys. Lett. **104**, 241604 (2014).
[15]J. J. J. Nivas, H. Shutong, K. K. Anoop, A. Rubano, R. Fittipaldi, A. vecchione, D. Paparo, L. marrucci, R. Bruzzese, and S. Amoruso, Opt. Lett. **40**, 4611 (2015).
[16]T. Omatsu, K. Chujo, K. Miyamoto, M. Okida, K. Nakamura, N. Aoki, and R. Morita, Opt. Express **18**, 17967 (2010).
[17]C. Hnatovsky, V. G. Shvedov, W. Krolikowski, and A. V. Rode, Opt. Lett. **35**, 3417 (2010).
[18]E. Stankevicius, T. Gertus, M. Rutkauskas, M. Gedvilas, G. Raciukaitis, R. Gadonas, V. Smilgevicius, and M. Malinauskas, J. Micromech. Microeng. **22**, 065022 (2012).
[19]B. Mills, D. Kundys, M. Farsari, S. Mailis, and R. W. Eason, Appl. Phys. A **108**, 651 (2012).
[20]G. Bautista, M. J. Romero, G. Tapang, and V. R. Daria, Opt. Commun. **282**, 3746 (2009).
[21]A. Ovsianikov, J. Viertl, B. Chichkov, M. Oubaha, B. MacCraith, I. Sakellari, A. Giakoumaki, D. Gray, M. Vamvakaki, M. Farsari, and C. Fotakis, ACS Nano **2**, 2257 (2008).
[22]A. S. van de Nes, L. Billy, S. F. Pereira, and J. J. M. Braat, Opt. Express **12**, 1281 (2004).
[23]H. Lin, B. H. Jia, and M. Gu, Opt. Lett. **36**, 406 (2011).
[24]X. Hao, C. F. Kuang, T. T. Wang, and X. Liu, J. Opt. **12**, 115707 (2010).
[25]M. A. A. Neil, R. Juskaitis, M. J. Booth, T. Wilson, T. Tanaka, and S. Kawata, Appl. Opt. **41**, 1374 (2002).
[26]L. Huang, P. S. Salter, F. Payne, and M. J. Booth, Opt. Express **24**, 10565 (2016).
[27]J. Hering, E. H. Waller, and G. Freymann, Opt. Express **24**, 28500 (2016).
[28]X. H. Tan, T. L. Shi, Y. Gao, W. J. Sheng, B. Sun, and G. L. Liao, J. Micromech. Microeng. **24**, 055006 (2014).
[29]W. Gao and J. Wang, ACS Nano **8**, 3170 (2014).
[30]Y. F. Mei, A. A. Solovev, S. Sanchez, and O. G. Schmidt, Chem. Soc. Rev. **40**, 2109 (2011).
[31]J. Fu, H. T. Dong, and W. Fang, Appl. Phys. Lett. **97**, 041114 (2010).
[32]D. J. Thurmer, C. Deneke, Y. F. Mei, and O. G. Schmidt, Appl. Phys. Lett. **89**, 223507 (2006).